Talanta 116 (2013) 1060–1066

Contents lists available at ScienceDirect

Talanta

journal homepage: www.elsevier.com/locate/talanta

Low-temperature synthesis of α-Fe_2O_3 hexagonal nanoparticles for environmental remediation and smart sensor applications

Ahmad Umar [a,b,*], M.S. Akhtar [c], G.N. Dar [a,d], S. Baskoutas [d]

[a] Promising Centre for Sensors and Electronic Devices (PCSED), Najran University, Najran-11001, P.O. Box-1988, Kingdom of Saudi Arabia
[b] Department of Chemistry, College of Science and Arts, Najran University, Najran-11001, P.O. Box-1988, Kingdom of Saudi Arabia
[c] New and Renewable Energy Materials Development Center (New REC), Chonbuk National University, South Korea
[d] Department of Materials Science, University of Patras, Rio Patras Gr-26504, Greece

ARTICLE INFO

Article history:
Received 1 July 2013
Received in revised form
13 August 2013
Accepted 15 August 2013
Available online 23 August 2013

Keywords:
α-Fe_2O_3 hexagonal nanoparticles
Rhodamine dye
Photo-degradation
4-Nitrophenol
Chemical sensor

ABSTRACT

This work demonstrates the successful synthesis and characterizations of α-Fe_2O_3 hexagonal nanoparticles and their effective utilization for the degradation of hazardous Rhodamine B (RhB) dye and smart chemical sensor applications. The as-synthesized materials were characterized by various analytical techniques which revealed that the prepared nanoparticles are well-crystalline, possessing hexagonal shape, grown in high-density and well matched with the rhombohedral α-Fe_2O_3 structures. The as-synthesized α-Fe_2O_3 nanoparticles were used as efficient photocatalyst for the photocatalytic degradation of RhB-dye under light illumination which showed substantial degradation (~79%) of RhB-dye in 140 min. The considerable photo-degradation of RhB-dye attributed to the unique morphology of the synthesized α-Fe_2O_3 nanoparticles which might import the effective electron/hole separation and generate the large number of oxy-radicals. Moreover, the synthesized α-Fe_2O_3 nanoparticles were utilized as efficient electron mediators for the fabrication of 4-nitrophenol chemical sensor in aqueous media. The fabricated chemical sensor exhibited a high-sensitivity of ~367.6 μA $(mol\ L^{-1})^{-1}\ cm^{-2}$ and an experimental detection limit of $\sim 1.56 \times 10^{-3}$ mol L^{-1} in a short response time of ~10.0 s with linearity in the range of 1.56×10^{-3}–12.5×10^{-3} mol L^{-1} and correlation coefficient (R) of ~0.99963. These investigations demonstrated that the simply synthesized α-Fe_2O_3 nanoparticles can effectively be used as efficient photocatalyst for the photocatalytic degradation of organic dyes and effective electron mediators for the fabrication of highly sensitive chemical sensors in aqueous medium.

1. Introduction

The residues of clothes and papers coloring industries are continuously accelerated by the water pollution. The coloring includes several hazardous organic compounds which cause the serious environmental problems to human health and the aquatic medium due to their toxicity and the carcinogenic effect [1–3]. These harmful dyes are majorly mineralized by the heterogeneous catalytic process including photocatalytic and chemical oxidation processes [1]. The photocatalytic decomposition by semiconductors nanomaterials has recently gained the most promising method for the decomposition/degradation of organic dyes in water to less harmful chemicals [4,5]. The metal oxides semiconductors are popularly employed as photocatalysts for the photocatalytic degradation of organic dyes owing to their wide band gap and high photosensitive nature [6–8]. An advance research is needed to develop efficient photocatalyst for the effective dye remediation.

On the other hand, the excess usage of the toxic chemicals as reacting species in most of the industries increases the environmental pollution [9,10]. Among various chemicals, the phenolic compound, 4-nitrophenol (4NP) is extensively used as intermediates in various manufacturing industries of pharmaceuticals, analgesics, pesticides, dyes, and processing of leather [11,12]. Recently, 4NP is listed in the Environmental Protection Agency List of Priority Pollutants due to its high toxicity to the environment and human [13–15]. Therefore, a rapid and fast environmental monitoring system or device is required to detect and quantify the concentration of hazardous 4NP chemical for avoiding the water pollution and untoward effects on human health. In this regards, recently, a solution processed Ce-doped ZnO nanorods based chemical sensor for the detection of phenol derivatives called hydroquinone that have been fabricated and reported in the literature [16]. J. Li et al. recently fabricated graphene oxide-based GC electrode based electrochemical sensor for the efficient

* Corresponding author at: Promising Centre for Sensors and Electronic Devices (PCSED), Najran University, Najran-11001, P.O. Box-1988, Kingdom of Saudi Arabia. Tel.: +966-534574597.
E-mail address: ahmadumar786@gmail.com (A. Umar).

0039-9140/$ - see front matter © 2013 Elsevier B.V. All rights reserved.
http://dx.doi.org/10.1016/j.talanta.2013.08.026

detection of 4NP chemical. Therefore, the metal oxides semiconductors such as TiO_2, ZnO, SnO_2 and Fe_2O_3 could be the appropriate materials for the photocatalytic degradation of organic dyes and smart sensing electrode for chemical sensor.

Among them, iron oxide (α-Fe_2O_3), hematite is recently receiving extensive attention as promising photocatalyst candidate due to its narrow band gap (2.0–2.2 eV) which could collect up to 40% of the solar spectrum energy, stability in most aqueous solutions and good magnetic properties [17]. Because of its excellent properties, to name a few, bio-compatible, thermodynamically stable, environmental friendly, low-synthesis cost, and so on, the α-Fe_2O_3 nanomaterials display the promising applications in several fields such as water splitting [18], sensors [19], Li-ion batteries and supercapacitors [20], photovoltaic [21], biomedical applications, etc. Recently, the utilization of α-Fe_2O_3 nanomaterials as photocatalyst has received great attention, especially for the degradation of harmful dyes and pollutants [22]. Importantly, it was examined that the performances of photocatalytic reactions are greatly influenced by particle size, shape and crystallinity of α-Fe_2O_3 nanomaterials [23]. The architectural aspects are still open to develop advance and efficient α-Fe_2O_3 nanomaterials for high performance photocatalytic reactions and highly sensitive system for the detection of hydroquinone chemical. Several efforts have been made to synthesize α-Fe_2O_3 nanostructures via sol–gel process [24], hydrothermal approach [25], and chemical precipitation [26], high energy ball milling [27] and so on.

In this paper, α-Fe_2O_3 hexagonal nanoparticles were synthesized, characterized and utilized as efficient photocatalysts for the degradation of hazardous Rhodamine B (RhB) dye and as effective electron mediators for the fabrication of highly sensitive 4NP chemical sensors in aqueous medium.

2. Experimental details

2.1. Synthesis of α-Fe_2O_3 hexagonal nanoparticles

α-Fe_2O_3 hexagonal nanoparticles were synthesized by the facile hydrothermal process using iron chloride hexahydrate ($FeCl_3 \cdot 6H_2O$) and hexamethylenetetramine (HMTA). In a typical reaction process for the synthesis of α-Fe_2O_3 nanoparticles, 0.05 mol L^{-1} $FeCl_3 \cdot 6H_2O$ was mixed with 0.03 mol L^{-1} HMTA in 50 ml DI water under vigorous stirring. Subsequently, few drops of $NH_3 \cdot H_2O$ was added in the resultant solution to make the solution of pH = 11 and stirred for 30 min. After stirring, the resultant solution was loaded into a Teflon-lined stainless steel autoclave, sealed it and heated up to 130 °C for 3 h. After completing the reaction, the autoclave was naturally cooled at room-temperature and finally dark brown product was obtained which was washed with DI water and ethanol sequentially. The obtained product was dried at 60 °C for 2 h. The synthesized products were examined in terms of their morphological, structural, photocatalytic and sensing properties.

2.2. Characterizations of as-synthesized α-Fe_2O_3 hexagonal nanoparticles

The as-synthesized α-Fe_2O_3 hexagonal nanoparticles were characterized in terms of their morphological, structural and optical properties. The general morphologies of as-synthesized nanoparticles are examined by field emission scanning electron microscopy (FESEM; JEOL-JSM-7600F) while the detailed morphological investigations were done by transmission electron microscopy (TEM) equipped with high-resolution TEM (HR-TEM). The crystallinity and crystal phases were examined by the X-ray diffraction (XRD; PANalytical Xpert Pro) pattern measured with Cu-Kα Radiation (λ = 1.54178 Å). The elemental and chemical compositions of as-synthesized α-Fe_2O_3 hexagonal nanoparticles were examined by energy dispersive spectroscopy (EDS) and Fourier transform infrared (FT-IR) spectroscopy, respectively. The scattering properties of as-prepared nanoparticles were examined by Raman-scattering spectroscopy.

2.3. Photocatalytic decomposition of Rhodamine B using as-synthesized α-Fe_2O_3 hexagonal nanoparticles

The photocatalytic degradation of RhB dye was carried out in a three neck pyrex flask reactor using α-Fe_2O_3 nanoparticles as photocatalyst under UV illumination of xenon arc lamp (300 W, Hamamatus: L2479). For the photocatalytic degradation of RhB dye, 10 ppm dye solution was prepared in 100 ml DI water in which 0.15 g photocatalyst (α-Fe_2O_3 nanoparticles) was added and the resultant mixture was purged with Ar gas under continuous stirring. Consequently, the obtained suspension was equilibrated for 30 min to stabilize the absorption of RhB dye over α-Fe_2O_3 nanoparticles prior to the light exposure. The photocatalytic degradation of the RhB dye was estimated by measuring the absorbance of dye solution in the presence of photocatalyst exposed at different time intervals (10 min). The absorbance was measured by UV–vis. spectrophotometer (Perkin Elmer-UV/vis-Lambda 950). The degradation rate of RhB dye was estimated according to the following equation [28,29]:

$$\text{Degradation rate } (\%) = (C_o - C/C_o) \times 100 = (A_o - A/A_o) \times 100$$

where C_o represents the initial concentration, C the variable concentration, A_o the initial absorbance, and A the variable absorbance.

2.4. Fabrication and characterization of 4-nitrophenol chemical sensor by I–V technique

For the fabrication of 4-nitrophenol chemical sensor, the glassy carbon electrode (GCE) was modified by using α-Fe_2O_3 hexagonal nanoparticles and used as working electrode. Prior to the modification, the surface of GCE was polished with alumina and thoroughly rinsed with DI water. To modify the electrode surface, slurry of α-Fe_2O_3 hexagonal nanoparticles were made by mixing an appropriate composition of nanoparticles and conducting agent (butyl carbitol acetate). Finally, a small amount of the slurry was casted on GCE (surface area 0.0316 cm^2) surface, and then the modified electrode was dried in electric oven at 60 ± 5 °C for 4 h. To investigate the sensor analytical performance, *I–V* technique was used as mentioned in the reported literature [9]. For *I–V* measurements; Zahner electrochemical workstation was used in which the α-Fe_2O_3 hexagonal nanoparticles/GCE was used as a working electrode while Pt wire was employed as a counter electrode. The current response was measured from 0.0 to 0.9 V while the time delaying and response time were 1.0 s and 10.0 s, respectively. For all the measurements, the amount of 10.0 mL phosphate buffer solution was kept constant. A wide concentration range (1.56×10^{-3} mol L^{-1} to 50×10^{-3} mol L^{-1}) was used for the concentration studies. All the sensing experiments were carried out at room-temperature.

3. Results and discussion

3.1. Morphological, structural and compositional properties of α-Fe_2O_3 hexagonal nanoparticles

The morphological and structural properties of as-synthesized iron oxide product was examined by FESEM and TEM and demonstrated in Fig. 1. Fig. 1(a) and (b) exhibits the typical FESEM

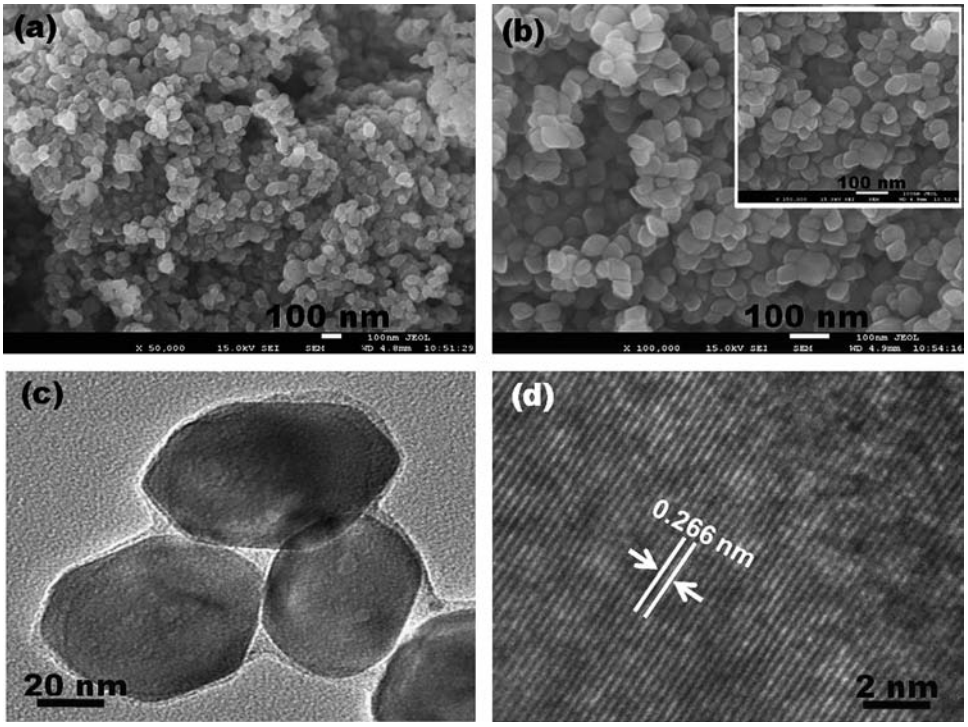

Fig. 1. Low (a) and (b) high-magnification FESEM images, (c) low and (d) high-resolution TEM images of as-synthesized α-Fe_2O_3 hexagonal nanoparticles.

images which reveal that the products are nanoparticles, prepared in large quantity and possessing hexagonal shape. The typical sizes of the nanoparticles are in the range of $\sim 30 \pm 10$ nm. The clear morphologies of as-prepared nanoparticles were examined by transmission electron microscopy (TEM) which reveals that the prepared material possesses well-defined hexagonal nanoparticles which are grown in high-density (Fig. 1(c)). The TEM image is fully consistent with observed FESEM images. The detailed structural properties of as-prepared nanoparticles were examined by high-resolution TEM (HRTEM) which confirms the high-crystalline nature of as-synthesized nanoparticles. The HRTEM image exhibits the well-defined lattice fringes which are separated by 0.266 nm and hence can be indexed to the (014) plane of the rhombohedral α-Fe_2O_3 structure.

The elemental compositions of as-prepared α-Fe_2O_3 nanoparticles was examined by EDS and shown in Fig. 2(a). The EDS spectrum revealed that the as-synthesized nanoparticles are composed of iron and oxygen. Moreover, no peak related with any impurity or other element is found in the spectrum which confirms that the synthesized nanoparticles are pure iron oxide without any significant impurity. The crystallinity and crystal phases of as-prepared nanoparticles were investigated by X-ray diffraction (XRD) (Fig. 2(b)). The XRD pattern was measured with Cu-Kα radiation ($\lambda = 1.54178$ Å) in the range of 10–70°. Several well-defined diffraction reflections are seen in the observed XRD pattern which is well matched to the rhombohedral α-Fe_2O_3 structures (JCPDS 84-0311). Due to sharp diffraction reflections, it can be concluded that the synthesized nanoparticles are well-crystalline. Except of rhombohedral α-Fe_2O_3 phase, no other reflection related with any impurity has been observed in the pattern which confirms that the as-synthesized products are pure and well crystalline.

The chemical composition of as-synthesized α-Fe_2O_3 nanoparticles was examined by FTIR measurement, carried out at room-temperature in the range of 430–4000 cm^{-1} (Fig.2(c)). Three well-defined absorption bands have been observed in the FTIR spectrum at 469, 575, and 3442 cm^{-1}. The appearance of two sharp absorption bands at 469 cm^{-1} and 575 cm^{-1} are due to the formation of Fe–O bonds which clearly confirmed the formation of iron oxide crystals [30]. The presence of vary short band at 3442 cm^{-1} is mainly because of the surface hydroxyl and O–H stretching mode which generally appeared when the FTIR measurements are done at room-temperature. Importantly, except Fe–O, no other significant absorption peak was seen in the spectrum which confirmed that the synthesized nanoparticles are highly pure iron oxide without any impurity.

Further to check the crystallinity, purity and scattering properties, the as-synthesized α-Fe_2O_3 nanoparticles were examined by Raman-scattering at room-temperature (Fig. 2 (d)). The α-Fe_2O_3 (hematite) belongs to D^6_{3d} crystal space group and group theory predicts seven phonon lines in the Raman spectrum [31]. Several well defined peaks at 225, 289, 403, 493, 608, and 1315 cm^{-1}were observed in the Raman-scattering spectrum which confirmed that the synthesized nanoparticles are pure α-Fe_2O_3. The peaks appeared at 225 and 608 cm^{-1} are assigned as Raman-active $A_{1g}(1)$ and $A_{1g}(2)$ modes, respectively. The appearances of other well-defined peaks at 289, 403, and 493 cm^{-1} are related with Raman-active E_g modes. A small and suppressed peak appeared at 1315 cm^{-1} is related with the second harmonic vibration mode.

3.2. *Photocatalytic degradation of Rhodamine B using α-Fe_2O_3 hexagonal nanoparticles*

The as-synthesized α-Fe_2O_3 nanoparticles were used as an efficient photocatalyst for the photocatalytic degradation of RhB dye under UV-light irradiation. The degraded RhB-dye over synthesized α-Fe_2O_3 nanoparticles was measured by UV–vis absorption spectra of centrifuged dye solution in every 10 min time interval, as shown in Fig. 3(a). The relative intensity of absorbance in UV–vis spectra is analyzed to estimate the percentage degradation of RhB dye. The strong absorbance at 554 nm in UV–vis has been observed by the degraded RhB-dye under UV light irradiation. The relative intensity of absorbance was continuously decreasing with increasing the exposure time of UV-light

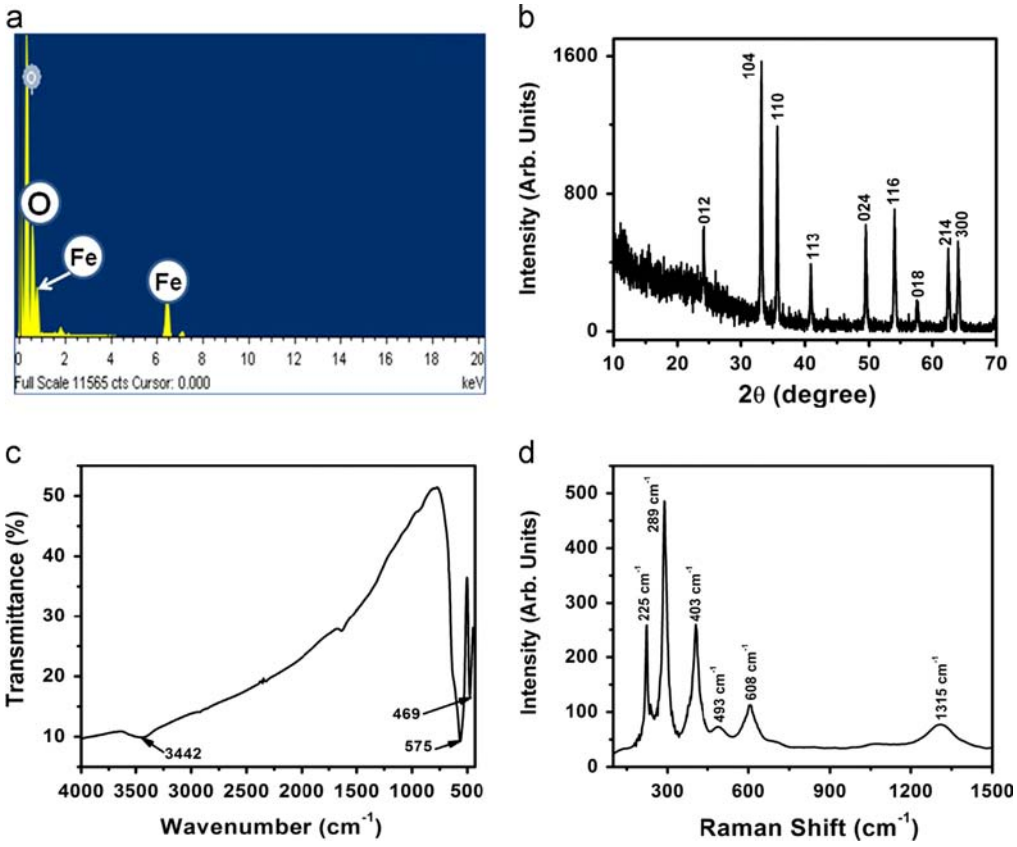

Fig. 2. (a) EDS spectrum, (b) XRD pattern, (c) FTIR spectrum and (c) Raman-scattering of as-synthesized α-Fe_2O_3 hexagonal nanoparticles.

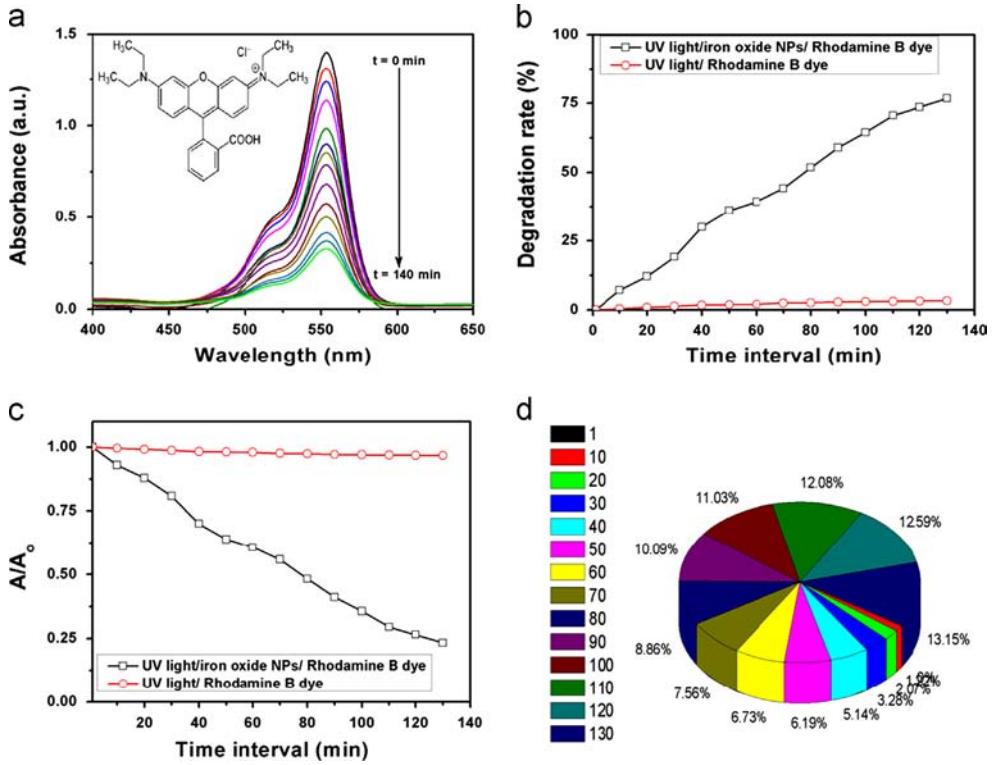

Fig. 3. (a) UV–vis absorbance spectra of decomposed RhB dye solution by light over as-synthesized α-Fe_2O_3 hexagonal nanoparticles, (b) degradation rate (%) and (c) extent of decomposition (A/A_o) of RhB dye with respect to time intervals, and (d) pie-diagram for the photocatalytic degradation of as-synthesized α-Fe_2O_3 hexagonal nanoparticles.

irradiation, indicating the continuous degradation of RhB-dye over the surface of synthesized α-Fe_2O_3 nanoparticles. It is estimated that the synthesized α-Fe_2O_3 nanoparticles substantially degraded the RhB dye by ~79% in 140 min.

Fig. 3(b) shows the plot of degradation rate versus time interval, and depicts the gradual increase of RhB-dye degradation rate under UV-light irradiation. Noticeably, a negligible degradation rate of RhB-dye is seen when photocatalytic reaction is performed under UV-light irradiation without α-Fe_2O_3 nanoparticles, confirms that degradation of RhB dye proceeds over the surface of α-Fe_2O_3 nanoparticles. Similar patterns have been observed in the plot of the variation in the relative concentration (A/A_o) versus time interval (Fig. 3(c)) for the degradation of RhB-dye over the surface of synthesized α-Fe_2O_3 nanoparticles under UV-light irradiation. Fig. 3(d) presents the pie chart of RhB-dye degradation which is evidenced that the most of RhB dye degradation is seen in 70 min over the surface of synthesized α-Fe_2O_3 nanoparticles. Thus, these results confirm the efficient RhB-dye degradation under UV-light illumination by synthesized α-Fe_2O_3 nanoparticles. Fig. 4 exhibits a schematic of RhB-dye degradation over the surface of α-Fe_2O_3 hexagonal nanoparticles under UV light illumination. Generally, the RhB-dye degradation could be explained by the separation of electron–hole ($\bar{e}$–h^+) pairs between the conduction (CB) and valence bands (VB) and high surface area of synthesized α-Fe_2O_3 nanoparticles. Moreover, during the separation of ($\bar{e}$–h^+) pairs, the formation of oxy-radicals such as hydroxyl ($OH^\bullet$)and superoxide ($O_2^\bullet$, $HO_2^\bullet$) are usually determined the degradation of organic dyes under light irradiation [32] which are generated on the surface of semiconductors [33].The following steps are involved for the generation of oxy-radicals during the photo-degradation of RhB-dye [34]:

$$\alpha - Fe_2O_3 + h\upsilon \rightarrow \alpha - Fe_2O_3(\bar{e}\text{–}h^+) \quad (1)$$

$$h^+ + H_2O \rightarrow {}^\bullet OH + H^+ \quad (2)$$

$$\bar{e} + O_2 \rightarrow O_2^- \quad (3)$$

$$O_2^- + H^+ \rightarrow HO_2^\bullet \quad (4)$$

$$O_2^- + RhB \rightarrow RhB^{+\bullet} - O_2 \quad (5)$$

$${}^\bullet OH + RhB^{+\bullet} \rightarrow CO_2 + H_2O \quad (6)$$

From the above steps, the high surface area of synthesized α-Fe_2O_3 nanoparticles sufficiently produces the active oxygen species {O_2, O_2^-, and $HOO^\bullet$/$^\bullet OH$} which are significantly responsible for high degradation of RhB-dye into less harmful organics. Therefore, the synthesized α-Fe_2O_3 nanoparticles with high surface exhibits the high degradation of RhB-dye under UV-light irradiation due to generation of $RhB^{+\bullet}$ and oxyradicals on the surface of synthesized α-Fe_2O_3 hexagonal nanoparticles.

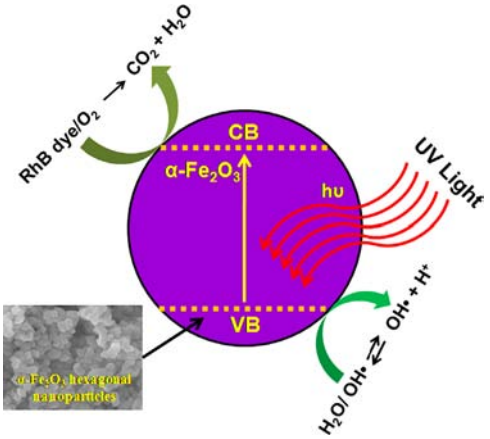

Fig. 4. A schematic of RhB dye degradation over the surface of as-synthesized α-Fe_2O_3 hexagonal nanoparticles under UV light illumination.

3.3. 4-Nitrophenol chemical sensor application of α-Fe_2O_3 hexagonal nanoparticles

The current (I)–voltage (V) measurements of the fabricated 4NP chemical sensor are performed to evaluate the sensing properties such as sensitivity, detection limit and correlation coefficient. The fabricated 4NP chemical sensor is composed of α-Fe_2O_3 hexagonal nanoparticles electrode as working electrode and Pt wire as counter electrode in 0.1 M phosphate buffer solution (PBS). From Fig. 5(a), a large increment in current is detected after addition of 4NP in PBS, whereas a low current is observed by sensor without 4NP chemical, which suggests that α-Fe_2O_3 hexagonal nanoparticles based electrode is highly active to 4NP chemical. Fig. 5 (b) shows a series of the I–V curves of the fabricated 4NP chemical sensor with α-Fe_2O_3 hexagonal nanoparticles based electrode to investigate the detail sensing behavior and parameters. The fabricated 4NP chemical sensor presents a continuous increase in current upon the incremental addition of 4NP with the concentrations range from $\sim 1.56 \times 10^{-3}$ mol L^{-1} to 50×10^{-3} mol L^{-1}. The continuously increased current might arise from the formation of large number of ions and the heightening in the ionic strength of the solution with the addition of 4NP. A plot of calibrated current versus 4NP concentrations (Fig. 5(c)) is drawn to estimate the sensitivity of the fabricated 4NP chemical sensor. It is seen that the calibrated current linearly increases as increasing the 4NP concentrations from 1.56×10^{-3} mol L^{-1} to 50×10^{-3} mol L^{-1}. High reproducible sensitivity of ~367.6 μA $(\text{mol L}^{-1})^{-1}$ cm^{-2} and good detection limit of $\sim 1.56 \times 10^{-3}$ mol L^{-1} with correlation coefficient (R) of ~0.99963 and short response time (10 s) is attained by the fabricated 4NP chemical sensor with α-Fe_2O_3 hexagonal nanoparticles based electrode. A good linearity by the fabricated 4NP chemical sensor with α-Fe_2O_3 hexagonal nanoparticles based electrode is achieved in the range from $\sim 1.56 \times 10^{-3}$ mol L^{-1} to 12.5×10^{-3} mol L^{-1}. The high sensitivity of 4NP chemical sensor might be attributed to the highly active surface of α-Fe_2O_3 hexagonal nanoparticles based electrode which might have large number of oxygenated species over the surface of α-Fe_2O_3 hexagonal nanoparticles. In this regards, Fig. 6 exhibits the mechanistic illustration of fabricated 4NP chemical sensor with α-Fe_2O_3 hexagonal nanoparticles based electrode. In electrochemical sensor, the oxygenated species are initially adsorbed on the α-Fe_2O_3 hexagonal nanoparticles based electrode after dipping into PBS in the electrochemical system. Afterwards, the ionic species such as O^{2-} and O^- are formed after gaining the electrons from the conduction band of α-Fe_2O_3 hexagonal nanoparticles [35,36]. These ionic species react with 4NP chemicals and converts into 4-nitroso phenol which again extradites electron to the conduction band of in presence of α-Fe_2O_3 hexagonal nanoparticles. This phenomenon is significantly increased the current and decreased the resistance of α-Fe_2O_3 hexagonal nanoparticles based electrode due to fast conduction of electrons during the sensing measurements. The multiple I–V measurements are performed for three consecutive weeks to investigate the reproducibility and the stability of fabricated 4NP chemical sensor with α-Fe_2O_3 hexagonal nanoparticles based electrode. No significant drop is observed in the sensing parameters, indicating the long term stability of the fabricated 4NP chemical sensor and high stability of α-Fe_2O_3 hexagonal nanoparticles based electrode.

The fabricated 4NP chemical sensor exhibits better sensitivity and low-detection limit as compared to those phenol based chemical sensors reported in the literature fabricated based on

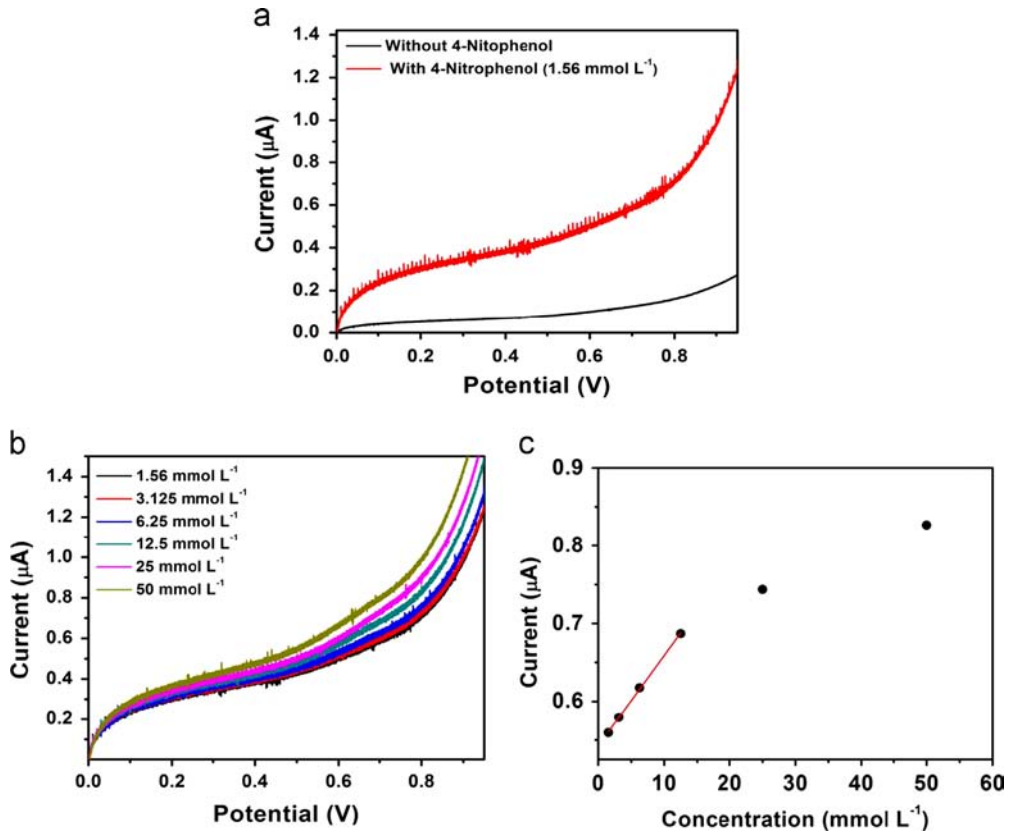

Fig. 5. (a) Typical *I–V* responses of α-Fe_2O_3 hexagonal nanoparticles modified GCE in 10 ml, 0.1 mol L^{-1} PBS solution, (Black line) without 4 nitro-phenol and (red line) with 4-nitro-phenol (1.56×10^{-3} mol L^{-1}); (b) *I–V* response for various concentrations of 4 nitro-phenol (from 1.56×10^{-3} mol L^{-1} to 50×10^{-3} mol L^{-1}) and (c) calibration curve. (For interpretation of the references to color in this figure legend, the reader is referred to the web version of this article.)

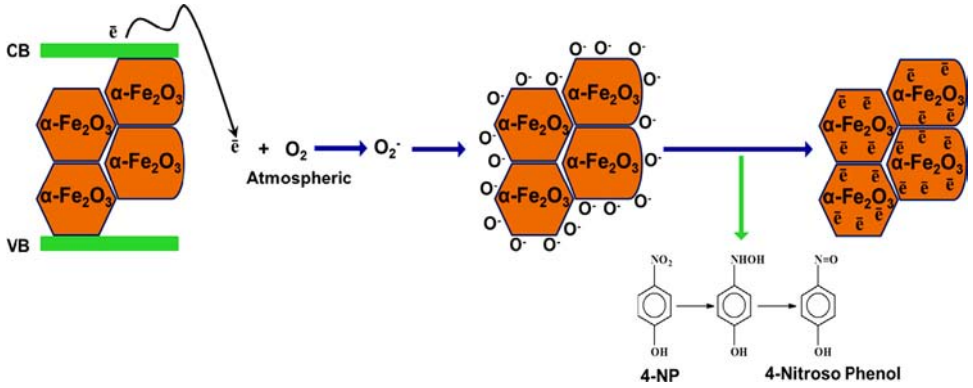

Fig. 6. Schematic representation of 4 nitro-phenol chemical sensor fabricated based on *I–V* technique using α-Fe_2O_3 hexagonal nanoparticles modified GC electrode as working electrode and chemical reaction describing the sensing mechanism.

Table 1
The comparison summary of the performances of 4-NP chemical sensors fabricated based on the utilization of various nanomaterials as electron mediators.

Materials	Limit of detection	Linearity	Correlation coefficient (R^2)	Sensitivity	Ref.
Pt/PEDOT-PB [a]	8.23 μmol L^{-1}	2–100 μmol L^{-1}	0.99108	0.116 μA/μmol L^{-1}	37
LiTCNE/GCE[b]	7.5 nmol L^{-1}	27–23,200 nmol L^{-1}	–	3.057 nA $nmol^{-1}$ cm^{-2}	38
Carbon nanotube modified electrode	4.0×10^{-7}	2.0 μmol L^{-1} to 4.0 mmol L^{-1}	–	–	39
HRP-TiO_2 nanotube[c]	2×10^{-7} mol L^{-1}	0.8–130 μmol L^{-1}	0.993	0.19 μA/μmol L^{-1}	40
α-Fe_2O_3 hexagonal nanoparticles/GCE	**1.56×10^{-3} mol L^{-1}**	**$1.56–12.5 \times 10^{-3}$ mol L^{-1}**	**0.99963**	**367.6 μA (mol L^{-1})$^{-1}$ cm^{-2}**	**This work**

[a] Poly(3,4-ethylenedioxythiophene) (PEDOT)/Prussian blue/polyazulene.
[b] Lithium tetracyanoethylenide/glassy carbon electrode.
[c] HRP=horseradish peroxidase.

nanomaterials based electrodes. Table 1 exhibits the comparison summary of the performances of 4-NP chemical sensors fabricated based on the utilization of various nanomaterials as electron mediators. It is apparent from Table 1 that the fabricated 4-NP chemical sensor based on α-Fe_2O_3 hexagonal nanoparticles exhibits better sensitivity and lower detection limit which confirms that the fabricated sensor is promising candidate for the effective detection of 4-NP. The sensing properties and parameters are comparable to reported literatures [37–40], as summarized in Table 1. Finally the high adsorption ability through the surface of α-Fe_2O_3 hexagonal nanoparticles results the efficient electrocatalytic activity towards 4NP chemical and exhibits the high sensitivity of the fabricated 4NP chemical sensor.

4. Conclusion

In summary, α-Fe_2O_3 hexagonal nanoparticles are synthesized by simple solution methods and applied as photocatalyst for the photocatalytic degradation of hazardous RhB-dye and as efficient electron mediator for the fabrication of effective 4-nitrophenol chemical sensor. By detailed morphological and compositional studies, it was confirmed that the as-synthesized α-Fe_2O_3 hexagonal nanoparticles possess well-crystalline, hexagonal disk shape and grown in high-density. The as-synthesized α-Fe_2O_3 nanoparticles were used as efficient photocatalyst and exhibit a substantial degradation (~79%) of RhB-dye in 140 min which was mainly due to specific morphologies of as-synthesized as it imports the effective electron/hole separation for the generation of the large number of oxy-radicals which contribute in the degradation process. The fabricated 4NP chemical sensor based on α-Fe_2O_3 hexagonal nanoparticles shows a high and reproducible sensitivity of ~367.6 μA $(mol\ L^{-1})^{-1}\ cm^{-2}$ and low-detection limit of $\sim 1.56 \times 10^{-3}\ mol\ L^{-1}$ with correlation coefficient (R) of ~0.99963 in a short response time (10 s). This work demonstrates that simply prepared α-Fe_2O_3 nanomaterials can efficiently be used as a photocatalyst for the photocatalytic degradation of organic pollutants and as effective electrode materials for the fabrication of highly sensitive sensor for the detection of hazardous and toxic chemicals.

Acknowledgment

This project was funded by the Deanship of Scientific Research (DSR), Najran University, Najran, under Grant no. NU-61/12. The authors, therefore, greatly acknowledge with thanks DSR, Najran University for technical and financial support.

References

[1] M.R. Hoffmann, S.T. Martin, W. Choi, D.W. Bahnemann, Chem. Rev. 95 (1995) 69–96.
[2] A. Khan, Niyaz A. Mir, M.M. Haque, M. Muneer, C. Boxall, Sci. Adv. Mater. 5 (2013) 160–165.
[3] Y. Zhu, X. Quan, F. Chen, X. Fan, Y. Feng, Sci. Adv. Mater. 4 (2012) 1191–1199.
[4] R. Kumar, G. Kumar, A. Umar, Mater. Lett. 97 (2013) 100–103.
[5] C. Cao, C. Hu, W. Shen, S. Wang, J. Wang, H. Liu, Y. Xi, Sci. Adv. Mater. 5 (2013) 796–802.
[6] S.A. Khayyat, M.S. Akhtar, A. Umar, Mater. Lett. 81 (2012) 239–241.
[7] C. Chen, H. Chen, J. Shi, J. Yu, Sci. Adv. Mater. 5 (2013) 896–903.
[8] C. Jin, C. Xing, F. Wang, W. Shen, Sci. Adv. Mater. 5 (2013) 663–667.
[9] G. Busca, S. Berardinelli, C. Resini, L. Arrighi, J. Hazardous Mater. 160 (2008) 265–288.
[10] K.-I. Choi, J.-H. Lee, Sci. Adv. Mater. 3 (2011) 811–820.
[11] H. Yin, Y. Zhou, S. Ai, X. Liu, L. Zhu, L. Lu, Microchim. Acta 169 (2010) 87.
[12] M. Castillo, R. Domingues, M.F. Alpendurada, D. Barcelo, Anal. Chim. Acta 353 (1997) 133.
[13] E. Lypczynska-Kochany, Chemosphere 22 (1991) 529–536.
[14] H. Ozay, Sci. Adv. Mater. 5 (2013) 575–582.
[15] M. Abaker, G.N. Dar, Ahmad Umar, S.A. Zaidi, Ahmed A. Ibrahim, A. BaskoutasS. Al-Hajry, Sci. Adv. Mater. 4 (2012) 893–900.
[16] G.N. Dar, A. Umar, S.A. Zaidi, A.A. Ibrahimd, M. Abaker, S. Baskoutas, M.S. Al-Assiri, Sens. Actuators B: Chem. 173 (2012) 72–78.
[17] D.K. Zhong, J.W. Sun, H. Inumaru, D.R. Gamelin, J. Am. Chem. Soc. 131 (2009) 6086–6087.
[18] I. Cesar, A. Kay, J.A. Gonzalez Martinez, M. Grätzel, J. Am. Chem. Soc 128 (14) (2006) 4582–4583.
[19] X. Li, W. Wei, S. Wang, L. Kuai, B. Geng, Nanoscale 3 (2) (2011) 718–724.
[20] J.S. Chen, T. Zhu, X.H. Yang, H.G. Yang, X.W. Lou, J. Am. Chem. Soc. 132 (38) (2010) 13162–13164.
[21] Y. Hou, D. Wang, X.H. Yang, W.Q. Fang, B. Zhang, H.F. Wang, G.Z. Lu, P. Hu, H.J. Zhao, H.G. Yang, Nat. Commun. 4 (2013) 1583.
[22] Z. Zhang, M.F. Hossain, T. Takahashi, Appl. Catal. B: Environ. 95 (2010) 423–429.
[23] X. Zhou, H. Yang, C. Wang, X. Mao, Y. Wang, Y. Yang, G. Liu, J. Phys. Chem. C 114 (40) (2010) 17051–17061.
[24] X. Wang, X. Chen, L. Gao, H. Zheng, M. Ji, C. Tang, T. Shen, Z. Zhang, J. Mater. Chem. 14 (2004) 905–907.
[25] C.J. Jia, L.D. Sun, Z.G. Yan, L.P. You, F. Luo, X.D. Han, Y.C. Pang, Z. Zhang, C.H. Yan, Angew. Chem. Int. Ed. 44 (2005) 4328–4333.
[26] X.Q. Su, B. Yan, Mater. Chem. Phys. 93 (2005) 552–556.
[27] L.L. Wang, J.S. Jiang, Physica B 390 (2007) 23–27.
[28] S.A. Khayyat, M. Abaker, A. Umar, M.O. Alkattan, N.D. Alharbi, S. Baskoutas, J. Nanosci. Nanotechnol. 12 (2012) 8453–8458.
[29] L.X. Zhang, P. Liu, Z.X. Su, Polym. Degrad. Stab. 91 (2006) 2213–2219.
[30] L. Chen, J. Zhang, Sci. Adv. Mater. 4 (2012) 859–862.
[31] S.P.S. Porto, R.S. Krishnan, J. Chem. Phys. 47 (1967) 1009–1012.
[32] D. Tassalit, A.N. Laoufi, F. Bentahar, Sci. Adv. Mater. 3 (2011) 944–948.
[33] L.S Roselin, R Selvin, Sci. Adv. Mater. 3 (2011) 251–258.
[34] V. Mirkhani, S. Tanngestaninejad, M. Moghadam, M.H. Habibi, A. Rostami Vartooni, J. Iran. Chem. Soc. 6 (2009) 578–587.
[35] P.P. Sahay, S. Tewari, S. Jha, M. Shamsuddin, J. Mater. Sci. 40 (2005) 4791–4793.
[36] F. Hellegouarch, F. Arefi-Khonsari, R. Planade, J. Amouroux, Sens. Actuators B: Chem. 73 (2001) 27–34.
[37] S. Lupua, C. Lete, M. Marin, N. Totir, P.C. Balaure, Electrochim. Acta 54 (2009) 1932–1938.
[38] R.S. Luz, F.S. Damos, A.B. Oliveira, J. Beck, L.T. Kubota, Talanta 64 (2004) 935–942.
[39] L. Luo, X. Zou, Y. Ding, Q. Wu, Sens. Actuators B: Chem. 135 (2008) 61–65.
[40] A.K.M. Kafi, A. Chen, Talanta 79 (2009) 97–102.